Journal of Alloys and Compounds, 184 (1992) 11–23
JALCOM 166

Model calculations for hydride nucleation on oxide-coated metallic surfaces: surface- and diffusion-related parameters

D. Cohen
Department of Nuclear Engineering, Ben-Gurion University of the Negev, PO Box 653, Beer-Sheva (Israel)

Y. Zeiri
Nuclear Research Center–Negev, PO Box 9001, Beer-Sheva (Israel)

M. H. Mintz
Department of Nuclear Engineering, Ben-Gurion University of the Negev, PO Box 653, Beer-Sheva (Israel) and Nuclear Research Centre–Negev, PO Box 9001, Beer-Sheva (Israel)

(Received October 3, 1991)

Abstract

In "real" metal–hydrogen systems the reacting metal (which is exposed to hydrogen at a given pressure and temperature) is initially coated by a thin passivation layer (referred to as an "oxide"). The initial penetration of hydrogen through this surface layer into the metal is a complex process consisting of different possible elementary steps. The nucleation of a hydride phase at the oxide–metal interface region initiates when the local concentration of hydrogen exceeds a certain solubility limit value. In the present work model calculations of the hydrogen concentration build-up at the oxide–metal interface were performed. In these calculations the permeation of hydrogen through the oxide was treated on a microscopic–atomic level, considering dissociative H_2 chemisorption on the surface, atomic hydrogen jumps between adjacent oxide atomic layers and hydrogen transitions across the oxide–metal interface. The respective set of coupled differential equations was solved numerically, yielding the corresponding hydrogen penetration flux across the interface. The subsequent diffusion process of hydrogen into the metal was treated on a macroscopic level, solving numerically a diffusion equation for a semi-infinite medium. These calculations yielded the time required for the build-up of the limiting concentration value (at the interface region), *i.e.* the so-called "nucleation induction period", as a function of the different dynamic parameters involved in the process (*e.g.* H_2 sticking probabilities, hydrogen jump rate constants and hydrogen diffusion constants in the metal). A detailed analysis of surface-related parameters and diffusion parameter effects is presented. The results are applied to account for the qualitative trends observed in the initial nucleation and growth stages of some metal–hydrogen reactions.

1. Introduction

In "real" metal–hydrogen systems the reacting metal (which is exposed to hydrogen at a given pressure and temperature) is usually coated by a thin non-metallic passivation layer referred to as an "oxide". This layer is formed by the reaction of the metal with the ambient atmosphere and besides oxygen may consist of additional elements, *e.g.* carbon and hydrogen. Thus the term "oxide" does not characterize accurately this layer, which may be

0925-8388/92/$5.00

composed of a mixture of real oxides, hydroxiles, oxicarbides and more. The composition of the layer and its thickness may also differ at different locations on the surface, *i.e.* display lateral as well as depth inhomogeneity. Owing to this inhomogeneity, the chemisorption of hydrogen on the "oxide" surface and its permeation rate through the layer into the metal may vary across the surface. Hence some locations on the "oxide" may be more "active" towards hydrogen than other locations, enabling a faster build-up of hydrogen concentration in the metal (near the oxide–metal interface). These locations may thus be preferred for the initial precipitation of a hydride phase (which precipitates when the local hydrogen concentration exceeds a certain solubility limit).

The existence of such oxide layers thus strongly affects the kinetics and morphology of hydride development, especially during the initial stages of the hydrogen–metal reactions. Two examples are given by vacuum heat pretreatments and gas phase impurities.

It is well known that vacuum heat treatments prior to the hydriding reactions greatly facilitate the initiation of these reactions. This effect has been reported for many metal–hydrogen systems, *e.g.* cerium [1], titanium [2] and uranium [3, 4].

The kinetic parameters which are most affected by these heat pretreatments are the initial induction times for the precipitation of the hydride and the nucleation rates. Higher pretreatment temperatures induce shorter induction periods and higher nucleation rates (*i.e.* producing a denser hydride "spot" pattern developing on the surface). In some cases not only are the nucleation parameters affected but also the growth rates of the hydride nuclei.

It has qualitatively been proposed [4] that the pronounced heat treatment effects on the nucleation parameters of the hydride are associated with surface modifications of the passivation layer, *e.g.* desorption of water. The outermost surface of the layer is then more active towards hydrogen, *i.e.* attains a higher sticking probability for hydrogen dissociative chemisorption, thus accelerating the accommodation of hydrogen at the "oxide"–metal interface and nucleation of the hydride.

Another example of "oxide"-related effects is given by the impediment to hydride nucleation and growth induced by impurities (*e.g.* O_2 and CO) existing in the reacting hydrogen gas (*e.g.* ref. 5 and references cited therein). These effects are also related to the chemisorption of the gas phase impurities on the surface of the coating oxide layers.

This view of the role of surface oxide layers, however, has not been substantiated so far by quantitative calculations to estimate the relative contribution of surface (chemisorption) and bulk (*e.g.* diffusion) effects on the initial nucleation process of hydrides on "oxide"-coated metals.

Some model calculations applying the atomistic picture of H_2 chemisorption and H atom permeation into the bulk have been presented in the literature [6, 7]. Nevertheless, the assumptions utilized in these calculations (*e.g.* steady state conditions and a homogeneous distribution of hydrogen in the metal) are not valid in the present case.

In the following sections a model describing the process of hydrogen concentration build-up at the oxide–metal interface is presented. The model couples a microscopic (atomistic) view of the chemisorption–oxide permeation steps with a macroscopic approach to hydrogen diffusion in the metal. The induction periods derived from the model are numerically calculated as a function of intrinsic rate parameters associated with the different elementary steps. In the present paper we focus on two rate parameters only, associated with surface chemisorption and with diffusion across the oxide. The sensitivity of the induction time values to variations in these parameters is checked and compared with observed experimental data.

2. The model

The precipitation of a hydride phase resulting from a gas–solid reaction occurs when the local concentration of hydrogen in the metal exceeds a certain value $C_s(T)$ referred to as the "solubility limit" (a temperature-dependent parameter). For an oxide-coated metal the build-up of hydrogen concentration near the oxide–metal interface involves a sequence of microscopic (atomic) elementary steps, starting with the dissociative chemisorption of H_2 on the oxide surface then surface-to-subsurface penetration, diffusion of H atoms through the oxide layer and H atom transitions across the oxide–metal interface. The hydrogen concentration in the metal near this interface is governed by the net difference in the fluxes of the incoming H atoms passing the oxide–metal boundary and the outgoing H atoms diffusing into the bulk of the metal.

In the following treatment we shall separate the dynamic problem into two parts.

(1) The sequence of elementary steps involved in the permeation process of hydrogen through the oxide layer: this part is treated on a microscopic (atomic) level within a simplified one-dimensional model.

(2) The diffusion of hydrogen into the bulk of the metal: this part is treated on a macroscopic level, solving the corresponding diffusion equation (assuming a semi-infinite medium).

These two parts are coupled through an oxide–metal boundary condition as described later.

Adapting a simplified picture, the oxide is visualized as being composed of n identical atomic layers, each separated by a distance δ_{ox}. The total thickness of the oxide is then given by

$$d_{ox} = (n-1)\delta_{ox} \tag{1}$$

The rate equation for hydrogen accommodation on the topmost surface layer (*i.e.* $n=1$) may be formulated by assuming a reversible dissociative chemisorption concomitant with reversible hydrogen fluxes into and from the subsurface region (*i.e.* the next atomic layer with $n=2$):

$$N_s \frac{d\theta_1}{dt} = J_{ads} - J_{des} - J_{12} + J_{21} \tag{2}$$

where θ_i is the fractional coverage of the ith layer, N_s is the maximum number of available hydrogen sites per unit area and the Js are the hydrogen fluxes associated with adsorption, desorption and layer $1 \leftrightarrow 2$ transitions respectively.

Assuming a random two-site Langmuir chemisorption, the adsorption and desorption fluxes may be given by

$$J_{ads} = 2k_g S_0(T) P(1-\theta_1)^2 \tag{3}$$

$$J_{des} = N_s k_{des}(T) \theta_1^2 \tag{4}$$

where k_g is the impingement rate constant given by the kinetic theory of gases (for H_2 and P expressed in Torr, $k_g = 2.48 \times 10^{22}/T^{1/2}$), $S_0(T)$ is the zero-coverage sticking probability (per impingement) for H_2 (at a given temperature T) and $k_{des}(T)$ is the desorption rate constant.

Similarly, the surface $\leftrightarrow$ subsurface (*i.e.* $1 \leftrightarrow 2$) fluxes may be formulated as

$$J_{12} = N_s k_{in}(T) \theta_1 (1-\theta_2) \tag{5}$$

$$J_{21} = N_s k_{out}(T) (1-\theta_1) \theta_2 \tag{6}$$

where k_{in} and k_{out} are the corresponding rate constants.

The diffusion of the H atoms within the oxide is approximated by assuming random jumps of H atoms between adjacent layers. Thus for the ith layer the fluxes between that layer and layers $i-1$ and $i+1$ are considered:

$$\frac{d\theta_i}{dt} = k_{i-1,i}(T)(1-\theta_i)\theta_{i-1} + k_{i+1,i}(T)(1-\theta_i)\theta_{i+1} - k_{i,i+1}(T)\theta_i(1-\theta_{i+1}) - k_{i,i-1}(T)\theta_i(1-\theta_{i-1}) \tag{7}$$

By approximating all the rate constants $k_{ij}(T)$ to be identical, *i.e.*

$$k_{ij}(T) = k_{ox}(T) = \frac{D_{ox}(T)}{\delta_{ox}^2} \tag{8}$$

eqn. (7) takes the form

$$\frac{d\theta_i}{dt} = k_{ox}(T)[(1-\theta_i)(\theta_{i-1}+\theta_{i+1}) - \theta_i(2-\theta_{i+1}-\theta_{i-1})] \tag{9}$$

(for $i = 2, 3, \ldots, n-1$). k_{ox} (s^{-1}) is the diffusion rate constant of hydrogen in the oxide and D_{ox} ($cm^2\ s^{-1}$) is the corresponding diffusivity.

For the last oxide layer (*i.e.* $i = n$) the forward jumps of H atoms are across the oxide–metal boundary. It is assumed that the potential barrier for backward jumps (*i.e.* metal $\rightarrow$ oxide) is much higher than that for forward jumps so that the reversible metal-to-oxide flux is negligible. Thus

$$\frac{d\theta_n}{dt} = -k_{om}(T)\theta_n(1-\theta_M{}^0) + k_{ox}(T)(1-\theta_n)\theta_{n-1} - k_{ox}(T)\theta_n(1-\theta_{n-1}) \quad (10)$$

where $k_{om}(T)$ is the rate constant for jumps across the oxide–metal interface and $\theta_M{}^0$ is the coverage of the first metal layer just beneath the nth oxide layer.

The flux of H atoms surmounting the oxide–metal boundary barrier is thus given by

$$J_{om}(t) = N_s k_{om}(T)\theta_n(t)[1-\theta_M{}^0(t)] \quad (11)$$

It is assumed that all the rate constants $k_j(T)$ in eqns. (4)–(11) follow an Arrhenius-type dependence

$$k_j(T) = \nu_j \exp\left(-\frac{E_j}{k_B T}\right) \quad (12)$$

where ν_j is a frequency factor, E_j is the activation energy barrier (for process j) and k_B the Boltzmann constant.

The values of the different kinetic parameters appearing in these equations can be estimated for some hydrogen–oxide systems. Typically the frequency factors are in the range 10^{12}–10^{13} s^{-1} and the activation barriers in the range 7–20 kcal mol^{-1} (0.3–1 eV). The sticking probability S_0 may vary by many orders of magnitude, ranging from high values (about 0.1) down to very low values which are below experimental detection limits (usually about 10^{-5}–10^{-6}). It is worth noting that the parameter which appears in eqn. (3) is not S_0 but rather the product S_0P. The conventional working pressures applied in hydriding experiments are about 10^3 Torr; hence the numerical range of S_0P has been chosen to be below 10^2.

The following part considers the (macroscopic) diffusion of hydrogen in the metal. We may approximate the metal as a semi-infinite medium (which is justified for oxide thicknesses much smaller than the thickness of the metal). The coupling of this bulk diffusion problem with the interface incoming flux (eqn. (11)) is analogous to the problem of gas phase dissolution in a semi-infinite medium [8].

The diffusion equation is

$$\frac{\partial C(X,t)}{\partial t} = D_m \frac{\partial^2 C(X,t)}{\partial X^2} \quad (13)$$

with the boundary conditions

$$\frac{\partial C(0,t)}{\partial X} = J_{om}(t) \quad (14)$$

$$C(X,0) = 0 \quad (15)$$

$$C(\infty,t) = 0 \quad (16)$$

where D_m is the diffusivity of hydrogen in the metal and $C(X, t)$ is the concentration of hydrogen at a distance X from the oxide–metal interface

at a given time t. It should be realized that $C(X, t)$ is given in volume concentration units whereas $N_s\theta_M{}^0$ in eqn. (11) is given in area concentration units. The following relation can then be applied to link these quantities:

$$C(0, t) = \frac{N_s\theta_M{}^0(t)}{\delta_m} \tag{17}$$

where δ_m is the average distance between two adjacent atomic layers in the metal.

The solution of eqns. (13)–(16) is given by [8]

$$C(X, t) = -\frac{1}{(4\pi D_m)^{1/2}} \int_0^t \frac{J_{om}(t')}{(t-t')^{1/2}} \exp\left(-\frac{X^2}{4D_m(t-t')}\right) dt' \tag{18}$$

The set of coupled equations (2)–(11), (17) and (18) was solved numerically using the third-order open Adams integrator [9] initiated by a fourth-order Runge–Kutta integrator for the solution of the differential equations (2)–(11), while eqns. (17) and (18) were solved using gaussian quadrature. This self-consistent scheme was applied for a given array of parameters characterizing the oxide thickness (n), its surface properties (S_0, k_{des}) its transport properties (k_{in}, k_{out}, k_{ox}), the oxide–metal interface properties (k_{om}), the metal properties (D_m, δ_m) and the working conditions (P, T). The time dependences of the hydrogen distribution in the oxide (*i.e.* $\{\theta_i(t)\}$) and in the metal (*i.e.* $C(X, t)$) are then obtained.

As stated before, the precipitation of a hydride phase first occurs within the near-interface region when the local concentration of hydrogen within that region exceeds the solubility limit $C_s(T)$. The time required for the build-up of this concentration (the so-called "induction time"), t_i, is then given by the condition

$$C(\epsilon, t_i) = C_s(T) \tag{19}$$

where ϵ is a small distance from the interface within which the hydride phase precipitation initiates.

3. Calculated results

3.1. Effects of diffusion-related parameters

By fixing the values of k_{in}, k_{out}, k_{om}, ϵ, D_m, C_s and S_0P, the induction time t_i can be calculated as a function of the two diffusion-related parameters of the oxide film, namely its thickness (or the number of layers composing the oxide, n) and its diffusion rate constant k_{ox}. A matrix of t_i (n, k_{ox}) values is then acquired.

It is more convenient to define a characteristic diffusion time τ_d as

$$\tau_d(n, k_{ox}) = \frac{n^2}{k_{ox}} \tag{20}$$

For higher τ_d values (*i.e.* thicker oxide films or slower diffusion rates in the oxide) the permeation process of hydrogen into the metal should be controlled mostly by the diffusion parameters; hence the induction time t_i should be proportional to τ_d. As τ_d decreases (*i.e.* faster diffusion), other rate constants start to make a significant contribution and the linear dependence of t_i and τ_d no longer holds.

The results of these calculations for a given set of parameters (summarized in Table 1) are presented in Fig. 1(A). The calculations were made for three chosen values of the chemisorption-related parameter S_0P. As indicated by Fig. 1(A), the above anticipated behaviour of t_i and τ_d is obeyed within a very wide range of S_0P values (covering more than six orders of magnitude in the range $S_0P = 10^2$–10^{-5} Torr). Within this S_0P range the dependence of t_i on τ_d is approximately linear for $\tau_d \gtrsim 200$. For this diffusion-controlled range the slope of log t_i *vs.* log τ_d is about 0.93, which is close to unity. On the other hand, for τ_d values below about 100 the dependence of t_i on τ_d becomes weaker, as expected when the diffusion is fast relative to other rate-controlling processes.

As S_0P decreases, surface chemisorption starts to dominate the hydrogen accommodation rate and the diffusion-controlled range is shifted to higher τ_d values, *e.g.* as demonstrated in Fig. 1(B) (for $S_0P = 10^{-10}$), where the log t_i *vs.* log τ_d plot yields a slope of about 0.8 within the τ_d range where a corresponding slope of about unity was displayed for the higher S_0P values.

3.2. *Effects of surface-related parameters*

The Langmuir-type two-site chemisorption model given by eqns. (3) and (4) leads to an equilibrium surface coverage given by

$$\theta_1(\mathrm{eq}) = \frac{k_a^{1/2}}{k_a^{1/2} + k_{des}^{1/2}} \tag{21}$$

with

$$k_a = \frac{2k_g S_0 P}{N_s} \tag{22a}$$

TABLE 1

Set of parameters utilized for the numerical calculations

Fixed parameters							
Parameter	k_{in}	k_{out}	k_{om}	ϵ	D_m	δ_m	C_s
Units	s^{-1}	s^{-1}	s^{-1}	cm	$cm^2\ s^{-1}$	cm	atoms cm^{-3}
Value	1	1	1	5×10^{-5}	10^{-9}	3×10^{-8}	1×10^{15}
Variables parameters							
Parameter		n			k_{ox}		S_0P
Units		Dimensionless			s^{-1}		Torr
Range		1–90			1–100		10^2–10^{-10}

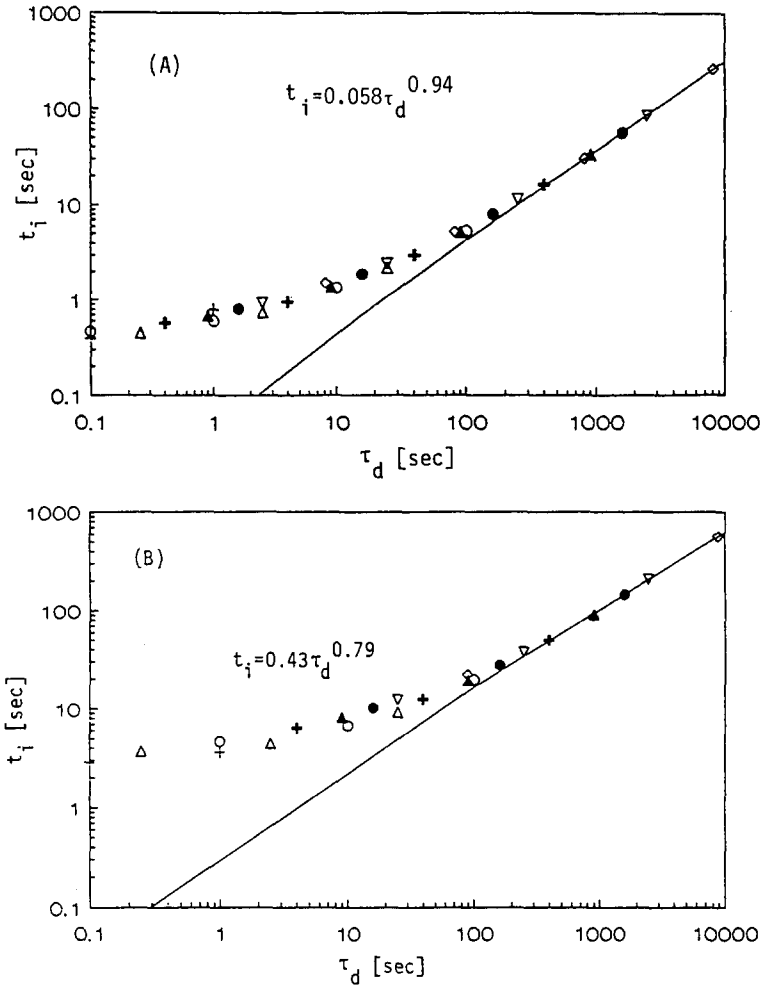

Fig. 1. Dependence of the hydride nucleation induction time t_i on the diffusion-related parameter $\tau_d = n^2/k_{ox}$: (A) $S_0P = 10^2$–10^{-5} Torr; (B) $S_0P = 10^{-10}$ Torr. (The different symbols represent different combinations of (n, k_{ox}); each symbol refers to a certain choice of n.) The set of rate parameters utilized in these calculations is given in Table 1. The solid lines represent the fitted relations indicated on each figure.

which for $N_s \approx 10^{15}$ sites cm^{-2} and k_g given by eqn. (3) (P given in Torr) assumes the form (at 300 K)

$$k_a \approx 2.9 \times 10^6 \times S_0P \tag{22b}$$

As long as k_a is much larger than the other rate constants, near-equilibrium surface coverage is attained much faster than the differential time step applied in the numerical solution of eqns. (7)–(11) and a time-independent value of θ_1 (eqn. (21)) can be utilized. On the other hand, when k_a is about equal

to or smaller than the other rate constants, eqn. (2) should be solved numerically, yielding the time dependence of $\theta_1(t)$. The non-equilibrium values of $\theta_1(t)$ are smaller than the equilibrium ones, *i.e.* $\theta_1(t) < \theta_1(\text{eq})$. In any case, as long as $k_a \gg k_{des}$, the θ_1 values are approaching a value close to unity and the change in S_0P within that range does not much affect the calculated results. This is illustrated in Fig. 2, where the calculated induction times t_i are plotted *vs.* S_0P for the same set of parameters given in Table 1 and for four values of the diffusion parameter τ_d (in the range 10^{-2}–8×10^3). It is seen that even though τ_d affects the absolute values of these curves, the qualitative trends are the same. In the range of S_0P where $k_a \gg k_{des}$ (which according to eqn. (22b) and Table 1 corresponds to $S_0P \gtrsim 10^{-6}$), t_i attains an almost constant value which is only very slightly affected by a change in S_0P. For lower S_0P values t_i starts to depend on this surface-related parameter, increasing with decreasing value of S_0P. It is possible to fit these curves to a phenomenological function of the type

$$t_i = A \exp\left(\frac{C}{(S_0P)^B}\right) \tag{23}$$

where A, B and C are constants (independent of S_0P). The fit of eqn. (23) to the calculated data is demonstrated in Fig. 2 by the solid curves. The values of the fitted parameters are summarized in Table 2. As $S_0P \to \infty$, $t_i \to A$. The parameter A is thus the asymptotic value of t_i when very fast surface chemisorption (relative to the other kinetic steps) takes place. The parameter A should then depend on the rate-limiting step dominating the permeation of hydrogen across the oxide, *e.g.* for large τ_d (diffusion controlled)

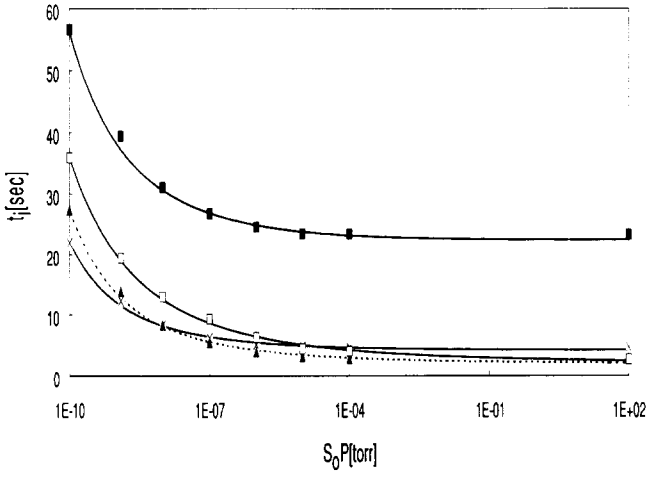

Fig. 2. Dependence of the hydride nucleation induction time t_i on the surface-related parameter S_0P: ▲, $\tau_d = 10^{-2}$ (displayed on the curve are the calculated t_i values multiplied by 10); ×, $\tau_d = 1$ (t_i values multiplied by 10); □, $\tau_d = 81$; ■, $\tau_d = 8100$ (t_i values divided by 10). The solid curves represent the fits of eqn. (23) to the calculated results. The fitting parameters A, B and C are summarized in Table 2.

TABLE 2

Fit of the parameters A, B and C (eqn. (23)) to the calculated data for different τ_d (or pairs of (n, k_{ox})) values

τ_d (s)	(n, k_{ox})	A (s)	B	C
10^{-2}	(1, 100)	0.20	0.13	0.12
1	(1, 1)	0.20	0.10	0.29
81	(90, 100)	4.16	0.19	0.02
8100	(90, 1)	2.24×10^{2}	0.23	4.3×10^{-3}

it should be affected by the diffusion-related parameter whereas for small τ_d it should no longer depend on this parameter. As seen from Table 2, these considerations are indeed fulfilled. The parameter A does not change much for τ_d in the range 10^{-2}–1 but increases by about an order of magnitude for τ_d in the range 81–8100. The other two parameters, B and C, are also summarized in Table 2. It seems that B is not sensitive to τ_d whereas C displays a complex dependence on the diffusion-related parameter. In any case it should be realized that the absolute values of these parameters (as well as the curves of t_i *vs.* S_0P) depend on the choice of the whole set of rate constants involved in the problem. For example, increasing the value of k_{des} results in a stronger variation in θ_1 starting at larger values of S_0P (according to eqns. (21) and (22)). Hence the sloping region in the t_i *vs.* S_0P curves will be displayed at larger S_0P values. Considering the possible range of the frequency pre-exponential factors and activation barriers (eqn. (12)), the possible range of the different rate constants under conventional working conditions (*e.g.* temperatures in the range 25–400 °C) is very wide (about 12 orders of magnitude, 10^{-2}–10^{10}). The present choice of these parameters only serves to demonstrate the qualitative behaviour of t_i given by a function of the type (23) and not the absolute values of the calculated results, as discussed further in the following section.

4. Discussion

As mentioned in Section 1, passivation films coating metal samples are non-uniform regarding both diffusion-related properties (d_{ox}, k_{ox}) and surface-related properties (S_0, k_{des}). In a simple manner, if a spread of Δk_j around a certain average $\bar{k}_j$ characterizes the film (with $\bar{k}_j$ either a surface- or bulk-related rate constant), the corresponding spread in nucleation times at different corresponding locations on the sample, Δt_i, should be proportional to the derivative $|(dt_i/dk_j)|_{\bar{k}_j}$. Hence, if $\bar{k}_j$ is located in a region where the slope of the t_i *vs.* k_j curve is steep, a wide spread in nucleation times is anticipated. On the other hand, the growth rates of the hydride are independent of the oxide-related parameter k_j, since whenever a hydride nucleus reaches a growth

stage, the oxide overlayer at that location had been ruptured [5]. Consequently, when the initial hydrogen–metal reaction is allowed to proceed to a certain extent (but still at a low reacted fraction), it is anticipated that a larger spread in Δt_i (resulting from a larger $|(dt_i/dk_j)|_{k_j}$) will produce a surface pattern with fewer (but larger) hydride "patches", whereas a smaller spread in Δt_i will display a pattern of dense (but small) hydride spots.

As stated before, vacuum heat treatments prior to the hydriding reactions result in shorter induction times and a denser pattern of hydride spots developing on the surface [4]. Conversely, the presence of gas impurities in hydrogen introduces longer induction times and hydride development characterized by the growth of a few "patches" [5]. Also, reducing the hydrogen working pressure results in conversion from a homogeneous surface reaction into a localized hydrogen attack at certain preferred spots [2].

It is evident from either Fig. 2 or the corresponding fit (eqn. (23)) that reducing the parameter S_0P shifts the derivative $dt_i/d(S_0P)$ into a steeper region. Actually, from eqn. (23)

$$\frac{dt_i}{d(S_0P)} = -\frac{ABC}{(S_0P)^{1+B}} \exp\left(\frac{C}{(S_0P)^B}\right) \tag{24}$$

or

$$\frac{1}{t_i}\frac{dt_i}{d(S_0P)} = \frac{d(\ln t_i)}{d(S_0P)} = -\frac{BC}{(S_0P)^{1+B}} \tag{25}$$

which indicates not only that dt_i becomes more sensitive to a reduction in S_0P (eqn. (24)) but also that the relative change dt_i/t_i attains a higher sensitivity to the variation in S_0P as this parameter decreases.

Vacuum heat pretreatments result in the desorption of chemisorbed species (*e.g.* water and OH), thereby increasing the specific reactivity of the oxide surface towards H_2 chemisorption (*i.e.* increasing the average value of S_0). Conversely, gas phase impurities which chemisorb on the surface reduce its activity. It is thus possible to account for all the experimentally observed effects described above by the theoretical behaviour anticipated for the corresponding charges in the parameter S_0P.

Among the three experimental effects described above (*i.e.* vacuum heat treatments, gas phase impurities and working pressure reduction), the first may be associated not only with changes in the surface-related parameters but also with alteration of the diffusion-related parameter τ_d. For example, slight changes in the stoichiometry of the oxide (*i.e.* its oxygen-to-metal ratio) resulting from these heat treatments may strongly affect the diffusion rate constant k_{ox}. As discussed in Section 3.1, for diffusion-controlled reactions t_i is proportional to τ_d (*i.e.* inversely proportional to k_{ox}). The relative sensitivity of t_i to a change in k_{ox} (*i.e.* $d(\ln t_i)/dk_{ox}$) is thus inversely proportional to that rate constant, increasing with decreasing value of k_{ox}. The observed effects of vacuum heat pretreatments may thus be associated also with the increased diffusivity induced by these treatments. On the other hand, effects of gas phase impurities or reduced working pressure are more likely to be

associated with the changes induced in the surface-related parameter S_0P only.

Finally, it is worthwhile to mention that the assumption utilized above, *i.e.* of an even spread of a given rate parameter Δk_j around an average value $\bar{k}_j$, is only a crude approximation introduced in order to simplify the above discussion. Actually, a certain non-even distribution exists regarding the area fraction characterized by a given value of k_j (or, more accurately, by a given interval between k_j and $k_j + dk_j$). Denoting this distribution function by $F(k_j)$, its relation to the corresponding induction time distribution function $F(t_i)$ (indicating the area fraction which reacts to form hydride nuclei in a time interval between t_i and $t_i + dt_i$) is given by the material (or area) conservation equation

$$F(k_j)\, dk_j = F(t_i)\, dt_i \tag{26}$$

The derivative dt_i/dk_j is thus involved in the transformation from the k_j space into the t_i space (the so-called jacobian of the transformation). It can be shown that for a given distribution $F(k_j)$, the larger $|(dt_i/dk_j)|_{\bar{k}_j}$ is, the broader is the $F(t_i)$ distribution.

This is illustrated in Fig. 3 for the surface-related parameter S_0P (eqn. (23)). Assuming a gaussian-type distribution for this parameter around a certain average $\overline{S_0P}$ and assuming the standard deviation $\sigma^2 = 0.1\overline{S_0P}$, the corresponding induction time distributions $F(t_i)$ are calculated for different values of the average $\overline{S_0P}$ (utilizing eqns. (23) and (26)). It is seen that even though $F(S_0P)$ is assumed to display a width which decreases with decreasing S_0P, the opposite trend is observed for $F(t_i)$, which broadens as $\overline{S_0P}$ is reduced.

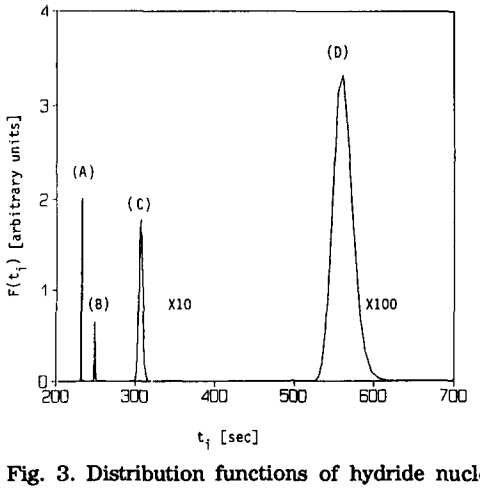

Fig. 3. Distribution functions of hydride nucleation times, $F(t_i)$, calculated from eqns. (23) and (26), assuming corresponding normal distribution functions of S_0P (around an average $\overline{S_0P}$ with a standard deviation given by $\sigma^2 = 0.1\overline{S_0P}$). The constants A, B and C in eqn. (23) were chosen from Table 2 (for $\tau_d = 8100$). (A) $\overline{S_0P} = 10^{-4}$ Torr; (B) $\overline{S_0P} = 10^{-6}$ Torr; (C) $\overline{S_0P} = 10^{-8}$ Torr; (D) $\overline{S_0P} = 10^{-10}$ Torr. The corresponding widths at half-maximum of $F(t_i)$ are (A) 0.45 s, (B) 1.47 s, (C) 5.26 and (D) 28.3 s.

In conclusion, the present model calculations provide a simple analytical relation (eqn. (23)) for the dependence of the hydride nucleation induction time t_i on the surface-related parameter S_0P. They also indicate that the sensitivity of t_i to variations in S_0P (and hence the spread in induction times associated with different nucleation locations on the heterogeneous surface) depends on the average value of this surface parameter (as well as on the spread of its distribution). For higher values of $\overline{S_0P}$ (resulting from either active oxide surfaces with high sticking probabilities or high hydrogen working pressures) a low $dt_i/d(S_0P)$ is anticipated, resulting in a hydride development morphology characterized by a dense pattern of growing hydride spots. For lower values of $\overline{S_0P}$ the sensitivity factor $dt_i/d(S_0P)$ increases steeply, resulting in a pattern of low density "patches" of growing hydrides.

A similar trend is obtained regarding the effects induced by changes in the diffusion-related parameters (for the diffusion of hydrogen in the oxide).

These calculations thus account for the experimentally observed behaviour of hydrogen–metal reactions in the initial stages of the hydriding process.

Acknowledgments

This work has been partially supported by a grant from the German–Israel Foundation (grant I-04-016.5/87) and partially by a grant from the Israel Council for Higher Education and the Israel Atomic Energy Commission.

References

1 K. H. Gayer and W. G. Bos, *J. Phys. Chem.*, *68* (1964) 2569.
2 A. Efrom, Y. Lifshitz, I. Lwekowicz and M. H. Mintz, *J. Less-Common Met.*, *153* (1989) 23.
3 J. Bloch, E. Swissa and M. H. Mintz, *Z. Phys. Chem. N.F.*, *164* (1989) 1193.
4 J. Bloch and M. H. Mintz, *J. Less-Common Met.*, *166* (1990) 241.
5 J. Bloch, D. Brami, A. Kremner and M. H. Mintz, *J. Less-Common Met.*, *139* (1988) 371.
6 M. A. Pick, J. W. Davenport, M. Strongin and G. J. Dienes, *Phys. Rev. Lett.*, *43* (1979) 286.
7 E. Fromm, H. Uchida and B. Chelluri, *Ber. Bunsenges. Phys. Chem.*, *87* (1983) 410.
8 J. F. D. Thuff and D. Naylor, *Differential Equations of Applied Mathematics*, Wiley, New York, 1966, p. 119.
9 R. W. Hornbeck, *Numerical Methods*, Quantum, New York, 1975.